Thermodynamics of lattice QCD with two light quarks on a $16^3 \times 8$ lattice. II

S. Gottlieb
Department of Physics, Indiana University, Bloomington, Indiana 47405

U. M. Heller and A. D. Kennedy
SCRI, The Florida State University, Tallahassee, Florida 32306-4052

S. Kim
Center for Theoretical Physics, Seoul National University, Seoul, Korea

J. B. Kogut
Department of Physics, University of Illinois, 1110 West Green Street, Urbana, Illinois 61801

C. Liu
Morgan Stanley and Co. Inc., 1585 Broadway, New York, New York 10036

R. L. Renken
Department of Physics, University of Central Florida, Orlando, Florida 32816

D. K. Sinclair
HEP Division, Argonne National Laboratory, 9700 South Cass Avenue, Argonne, Illinois 60439

R. L. Sugar
Department of Physics, University of California, Santa Barbara, California 93106

D. Toussaint
Department of Physics, University of Arizona, Tucson, Arizona 85721

K. C. Wang
China Graduate School of Theology, 5 Devon Rd, Kowloon Tong, Kowloon, Hong Kong
(Received 20 December 1996)

We have extended our earlier simulations of the high-temperature behavior of lattice QCD with two light flavors of staggered quarks on a $16^3 \times 8$ lattice to a lower quark mass ($m_q = 0.00625$). The transition from hadronic matter to a quark-gluon plasma is observed at $6/g^2 = 5.49(2)$ corresponding to a temperature of $T_c \approx 140$ MeV. We present measurements of observables which probe the nature of the quark-gluon plasma and serve to distinguish it from hadronic matter. Although the transition is quite abrupt, we have seen no indications that it is first order. [S0556-2821(97)05011-X]

PACS number(s): 12.38.Gc, 11.15.Ha

I. INTRODUCTION

The understanding of the thermodynamics of hadronic matter is a major goal of lattice QCD. In particular, one would like to find and understand the nature of the transition from hadronic matter to a quark-gluon plasma and to determine the properties of this plasma phase which serve to distinguish it from the hadronic phase. Such high-temperature matter must surely have existed in the early universe, and its properties would have helped determine the evolution of the Universe. In addition, it is believed that heavy-ion collisions such as will be observed at the BNL Relativistic Heavy Ion Collider (RHIC) will produce hot nuclear or hadronic matter and probably quark-gluon plasma. Finally, such studies can help us understand the dynamics of QCD including confinement and chiral symmetry breaking.

We have carried out simulations of QCD with two flavors of light-staggered quarks on a $16^3 \times 8$ lattice. In the first paper in this series we described simulations with quark mass $m_q = 0.0125$, in lattice units [1]. In the current paper we describe simulations with quark mass $m_q = 0.00625$ and, where possible, attempt to extrapolate to the chiral limit. Prior results of this study were reported at lattice conferences [2,3], and there has also been a report from the Columbia group on their work with a lighter quark mass, 0.004 [4].

The simulations were performed on the Connection Machine (CM-2) at the Pittsburgh Supercomputing Center. We used the hybrid molecular dynamics algorithm with noisy fermions for our simulations enabling us to tune the number of quark flavors to 2. As at the higher mass, we found no evidence for a first-order transition, in agreement with work on lattices with $N_t = 4$ [5], 6 [6], and 12 [7]. This is what was predicted on the basis of chiral spin models, which predict a second-order transition at $m_q = 0$ and a rapid crossover, with no transition at small m_q [8].

The position of the transition was determined by measuring the Wilson-Polyakov line, which is associated with confinement, and the chiral condensate $\langle\overline{\psi}\psi\rangle$, which measures chiral symmetry breaking. In addition, we have calculated the entropy densities of both quarks and gluons, and measured the topological susceptibility. From the correlation functions of spatial and temporal Wilson lines, we have estimated the string tensions and Debye screening lengths, and addressed the question of ψ/J production. By measuring the baryon number susceptibility, we have determined how the system responds to a finite chemical potential for baryon number. Additionally, we have measured the hadronic screening lengths for light hadronic excitations. These should give us an indication as to whether the plasma has any hadronlike excitations or whether its excitations are simply quarks and gluons. Finally, we have added valence ''strange'' quarks, whose masses are tuned to give the correct kaon masses when combined with u or d quarks of mass $m_q=0.00625$. By measuring the entropy of such strange quarks, we can address the question as to whether the formation of the quark-gluon plasma is characterized by increased kaon production. We have also measured the kaon screening lengths.

Section II describes the simulations and the extractions of most of the order parameters. In Sec. III we discuss Debye and hadronic screening lengths. Finally, in Sec. IV we present further discussions and conclusions.

II. SIMULATIONS

These simulations were performed on a $16^3\times 8$ lattice with 2 flavors of light quarks with mass $m_q=0.00625$, which will be compared, when appropriate, with earlier simulations with $m_q=0.0125$ [1]. The updating was performed with time increment $dt=0.005$, except at $6/g^2=6.0$ and the first half of the simulations at $6/g^2=5.55$ where it was chosen to be $dt=0.01$. We have simulated for 1000 time units at $6/g^2=5.45$, 1500 time units at $6/g^2=5.475$, 1145 time units from a cold start, and 1000 time units from a hot start at $6/g^2=5.5$, and 1000 time units at each of $6/g^2=5.525$, 5.55, and 6.0. Configurations were saved every 20 time units at $6/g^2=6.0$, every 10 time units at $6/g^2=5.55$, and every 5 time units for each of the other couplings. These configurations were used for later analyses.

The thermal (temporal) Wilson-Polyakov line, and the chiral condensate $\langle\overline{\psi}\psi\rangle$ were measured and are plotted in Fig. 1. They are tabulated, along with values of the plaquette, in Table I. In each case the first 200 time units are discarded for equilibration. The rapid crossover of these two quantities between $6/g^2=5.475$ and $6/g^2=5.5$ suggests that the transition occurs in this range. This is further borne out by looking at the time histories of the Wilson-Polyakov line at $6/g^2=5.475$ and 5.5. These are shown in Fig. 2. At $6/g^2=5.5$, starts from both the hot and cold sides of the transition evolve to the high-temperature phase. At $6/g^2=5.475$, starting from the high temperature phase, the system rapidly settles into the low temperature phase and stays there.

We have measured the partial entropy densities for the gluons and the light dynamical (u and d) quarks. In addition, we have calculated the partial entropy densities for a heavier

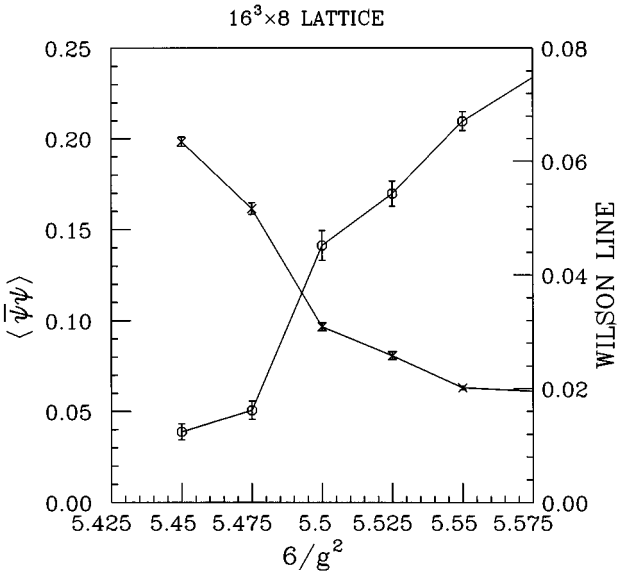

FIG. 1. The Wilson-Polyakov line (circles) and $\langle\overline{\psi}\psi\rangle$ (crosses) as functions of $6/g^2$.

''strange'' (s) valence quark. At tree order the partial entropies for the quarks and gluons are given by

$$s_g^0 T=\frac{4}{g^2}(P_{st}-P_{ss}) \tag{1}$$

and

$$s_f^0 T=\frac{n_f}{3}[\langle\overline{\psi}\not{D}_0\psi\rangle-\tfrac{3}{4}+\tfrac{1}{4}m_q\langle\overline{\psi}\psi\rangle], \tag{2}$$

respectively, where P_{st} and P_{ss} are the space-time and space-space plaquettes normalized as in [1]. Since at this order, the energy density ϵ and pressure p obey the perfect gas relation $p=\frac{1}{3}\epsilon$, which is clearly false for a first-order transition, we include the one-loop corrections. Through one-loop order [9],

$$s_g T=\left(1-\frac{1.279}{6/g^2}\right)s_g^0 T, \tag{3}$$

$$s_f T=\left(1-\frac{1.022}{6/g^2}\right)s_g^0 T. \tag{4}$$

TABLE I. The Wilson-Polyakov line and $\langle\overline{\psi}\psi\rangle$ as functions of $6/g^2$ for $m_q=0.00625$.

$6/g^2$	Wilson line	$\langle\overline{\psi}\psi\rangle$	Plaquette
5.45	0.0124(14)	0.1983(25)	0.45780(11)
5.475	0.0162(16)	0.1615(32)	0.45328(12)
5.5	0.0452(26)	0.0966(21)	0.44850(9)
5.525	0.0543(22)	0.0806(21)	0.44493(9)
5.55	0.0671(17)	0.0630(10)	0.44099(7)
6.0	0.2067(24)	0.02925(3)	0.39243(3)

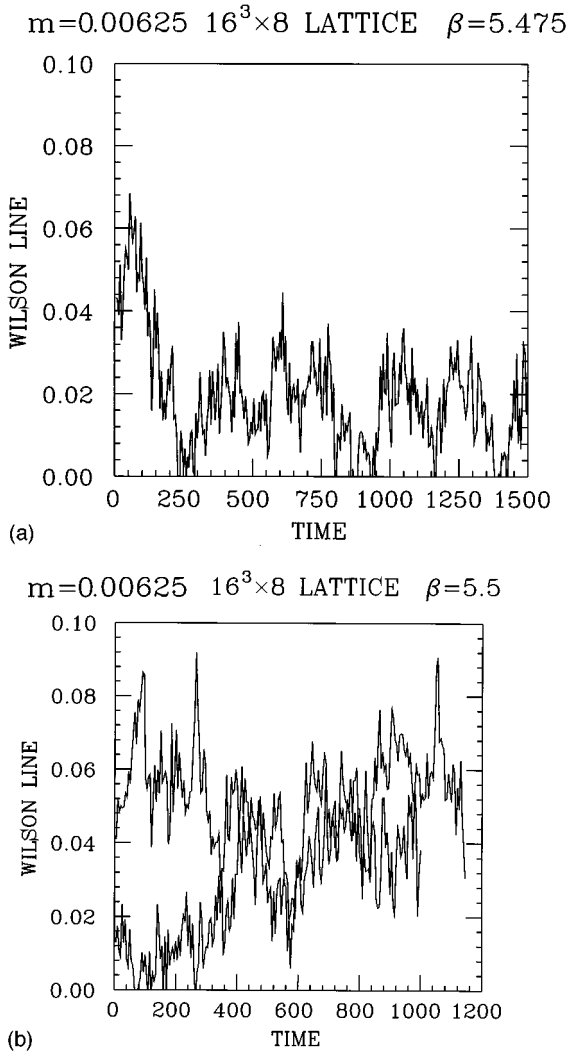

FIG. 2. Time evolution of the Wilson-Polyakov line (a) at $6/g^2=5.475$ and (b) at $6/g^2=5.5$.

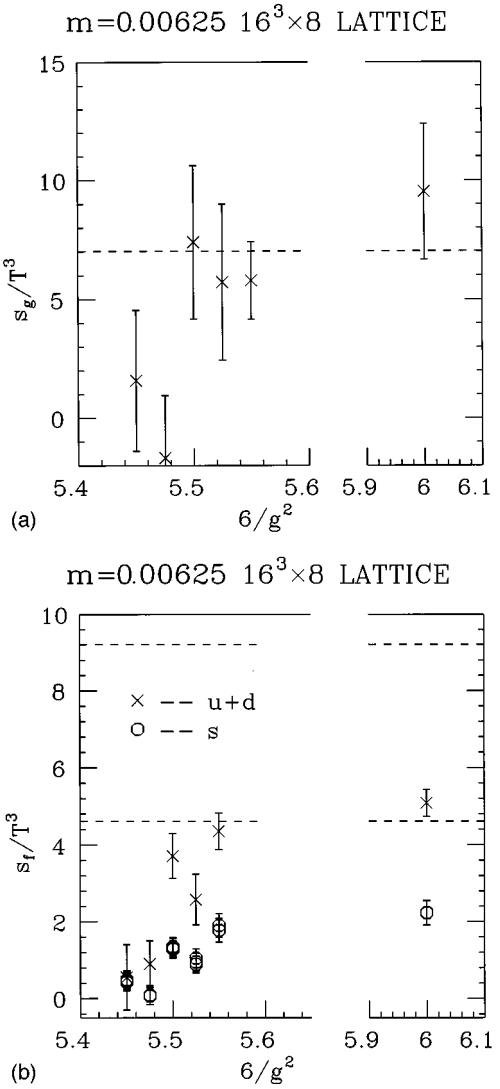

FIG. 3. Partial entropy densities of (a) the gluons and (b) the quarks as function of $6/g^2$. The dashed lines are the Stefan-Boltzmann values, in (b) the lower dashed line is for the s quarks and the upper is for the $u+d$ quarks.

The tree-level quantities are tabulated in Table II. The multiple values for the strange quark at each $6/g^2$ correspond to different choices for the strange quark mass, which span the range of estimates for the masses required to give the correct kaon mass when $m_{u,d}=0.00625$. The values chosen were 0.035, 0.040, 0.045, and 0.050 at $6/g^2=5.45$; 0.030, 0.035, and 0.040 at $6/g^2=5.475$; 0.025, 0.030, and 0.035 at $6/g^2=5.5$; 0.020, 0.025, and 0.030 at $6/g^2=5.525$; 0.0175, 0.0225, and 0.0275 at $6/g^2=5.55$; and 0.010 and 0.015 at $6/g^2=6.0$. The one-loop-corrected partial entropy densities, each divided by the ratio of the corresponding free field quantity on a $16^3\times 8$ lattice to its continuum value, in an attempt to remove some of the finite-size and finite lattice spacing effects [10], are plotted in Fig. 3. The above ratios are 0.99136 for gluons and 1.59828 for u and d quarks. The gluon partial entropy density divided by T^4 is small for small values of $6/g^2$, and increases abruptly to close to the Stefan-Boltzmann value $(32\pi^2/45)$ between $6/g^2=5.475$ and $6/g^2=5.5$, and remains there as $6/g^2$ is increased. The partial

TABLE II. Partial entropy densities for gluons, u plus d quarks, and s quarks at the tree order.

$6/g^2$	s_g^0/T^3	s_{u+d}^0/T^3	s_s^0/T^3			
5.45	1.9(3.6)	1.2(1.8)	1.0(5)	1.0(5)	0.9(5)	0.9 (5)
5.475	−2.1(3.2)	1.9(1.2)	0.2(5)	0.2(5)	0.1(5)	
5.5	9.0(3.9)	7.7(1.2)	2.8(5)	2.7(5)	2.6(5)	
5.525	7.0(4.0)	5.0(1.4)	2.1(5)	2.0(5)	1.8(5)	
5.55	7.0(3.5)	8.8(0.9)	3.9(6)	3.7(6)	3.7(6)	
6.0	11.3(3.4)	10.2(0.7)	4.5(7)	4.5(7)		

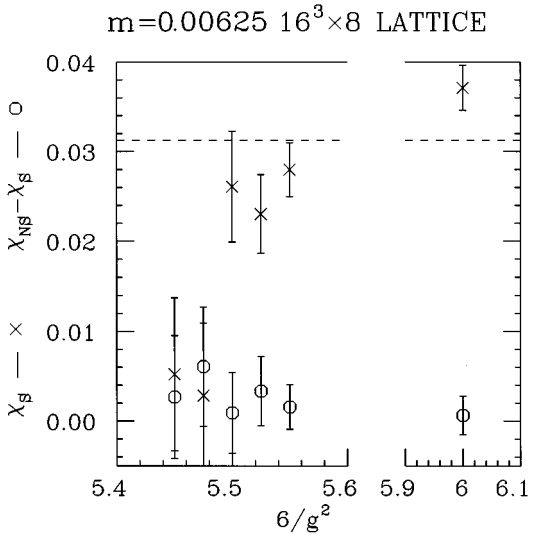

FIG. 4. Quark-number susceptibility χ_S and $\chi_{NS}-\chi_S$ as functions of $6/g^2$.

entropy density for the $u+d$ quarks over T^3 also increases rapidly between $6/g^2=5.475$ and $6/g^2=5.5$, and slowly increases for higher values. Even by $6/g^2=6.0$, it is still little more than one-half its Stefan-Boltzmann value ($7\pi^2 n_f/15$). This slow approach to its asymptotic value could well be due to poor convergence of the perturbative loop expansion. However, in contrast with the case of Wilson fermions, tadpole improvement is not expected to be (and in fact is not) of any help [11]. The entropy density of the strange quark behaves in a fashion qualitatively similar to that of the $u+d$ quarks. Just above the transition (at $6/g^2=5.5$), it is about 36% of that of the $u+d$ quarks, while by $6/g^2=6.0$ it has risen to about 44% on its way to the high-temperature limit of 50%.

For a complete understanding of the thermodynamics of lattice QCD one really needs to work at finite baryon- and hence quark-number density. Although that is beyond the scope of these simulations, we have measured the singlet (S) and nonsinglet (NS) quark-number susceptibilities [12],

$$\chi_S=\left(\frac{\partial}{\partial\mu_u}+\frac{\partial}{\partial\mu_d}\right)(\langle n_u\rangle+\langle n_d\rangle) \tag{5}$$

and

$$\chi_{NS}=\left(\frac{\partial}{\partial\mu_u}-\frac{\partial}{\partial\mu_d}\right)(\langle n_u\rangle-\langle n_d\rangle), \tag{6}$$

where $\langle n_u\rangle$ and $\langle n_d\rangle$ are the expectation values of the number densities for u and d quarks and μ_u and μ_d are chemical potentials for u and d quarks. We have evaluated χ_S and χ_{NS} on the lattice evaluated at zero chemical potentials using the method of [12] with 50 noise vectors (except at $6/g^2=5.55$ where we used 20, 50, and 100 noise vectors, we report results only for 100 noise vectors, which indicated that 50 noise vectors were adequate), and plotted our results in Fig. 4. The difference between χ_{NS} and χ_S remains small throughout the range. χ_S is small below the transition, rising rapidly to close to the continuum limit, $N_f T^2=0.03125$, as $6/g^2$ is increased through the transition, exceeding the continuum value for large $6/g^2$, a possible finite-size effect. The singlet susceptibility measures the ease with which a quark excess can be created by a finite chemical potential. Below the transition, confinement prevents the production of quarks, except as baryons, which requires extra energy: thus χ_S is small. Above the transition unconfined quarks can be created, which requires little energy, so χ_S is large. χ_{NS} measures the ease with which an excess of u quarks and anti-d quarks can be created. Below the transition, the easiest way to do this is to create an excess of π^+'s. However, the mass of the pion (larger than normal since m_q is larger than its physical value) tends to suppress such production, and χ_{NS} is small. Above the transition u and $\bar{d}$'s can be created with little energy and χ_{NS} is large.

Quark-number susceptibility is just one of the quantities which is of importance if our eventual goal is to understand the equation of state near the transition. Other such quantities are the fluctuation quantities such as [13,14]

$$C_V=\frac{1}{VT^2}\frac{\partial^2}{\partial(1/T^2)}\ln Z, \tag{7}$$

$$\chi_m=\frac{T}{V}\frac{\partial^2}{\partial m_q^2}\ln Z, \tag{8}$$

$$\chi_t=\frac{T}{V}\frac{\partial^2}{\partial m_q\partial(1/T)}\ln Z. \tag{9}$$

Since such quantities have peaks which span only a small range of $6/g^2$, to calculate them directly requires knowing their values at $6/g^2$'s which are closer together than typically simulated. This deficiency can often be overcome by interpolating using the Ferrenberg-Swendsen [15] method. We found, unfortunately, that the spacing of our simulated $6/g^2$'s, $\Delta 6/g^2=0.025$ in the transition region, was too large to permit such an interpolation. We estimate that one would need a $\Delta 6/g^2\approx 0.01$ (or less) to enable such an interpolation on this size lattice (not unreasonable for future simulations). The contributions to these quantities at only the simulated values of $6/g^2$ show little variation, and no peaks, the transition region is too narrow and none of our points is close enough to feel much effect. In the case of χ_m, since only one noise vector was used for each estimate of $\langle\bar{\psi}\psi\rangle$, it is probable that the fluctuations from use of this stochastic estimator completely overwhelmed those associated with the gauge configurations [16].

From our measurements of the Wilson-Polyakov line, $\langle\bar{\psi}\psi\rangle$ and entropy density, we conclude that the transition from hadronic matter to a quark-gluon plasma occurs at $6/g^2=5.49(2)$ for $m_q=0.00625$ as compared to $6/g^2=5.54(2)$ for $m_q=0.0125$. Linear extrapolation leads us to predict that the transition would occur at $6/g^2=5.44(3)$ in the chiral ($m_q=0$) limit. This m_q dependence of the position of the phase transition makes it difficult to extrapolate observables to $m_q=0$, since to extrapolate to $m_q=0$ at constant $6/g^2$ requires $6/g^2$ to lie on the same side of the transition at $m_q=0$ as that at $m_q=0.0125$. Of course, one might argue that it is more physical to continue, not at constant $6/g^2$ but rather at constant physics. Since the change in $6/g^2$ for the

TABLE III. $\langle\overline{\psi}\psi\rangle$ extrapolated to $m_q=0$. Those values marked with an asterisk are not to be interpreted as true $m_q=0$ values, but are included because they are related to topological charge. Naive extrapolations which cross the transition are included in square brackets for comparison.

	$\langle\overline{\psi}\psi\rangle$		
$6/g^2$	$\Delta(6/g^2)=0.000$	$\Delta(6/g^2)=0.025$	$\Delta(6/g^2)=0.050$
5.400			0.2161(56)
5.425			0.1660(67)
5.450	0.1420(58)*	0.1425(68)*	0.0785(44)
5.475			0.0584(43)
5.500	[0.0126(49)]	0.0467(23)	0.0285(24)
5.525	[0.0043(47)]	0.0230(23)	
5.550	0.0113(23)		
6.000	0.00011(9)		

transition $\Delta(6/g^2)\approx 0.05$ between $m_q=0.00625$ and $m_q=0.0125$ and between $m_q=0$ and $m_q=0.00625$, we have attempted linear extrapolations in mass with $\Delta(6/g^2)=0.05$ between $m_q=0.00625$ and $m_q=0.0125$ as well as for the traditional $\Delta(6/g^2)=0$. In addition, we have included extrapolations for $\Delta(6/g^2)=0.025$. Such extrapolations are shown for the chiral condensate $\langle\overline{\psi}\psi\rangle$ in Table III. Except at $6/g^2=5.45$, we have restricted ourselves to those for which the $m_q=0.0125$, the $m_q=0.00625$, and $m_q=0$ lie on the same side of the transition. At $6/g^2=5.45$, we have included cases where the $m_q=0.0125$ and $m_q=0.00625$ points lie in the hadronic phase while the $m_q=0$ point (probably) lies in the plasma phase. Although not representing the correct chiral limit, these, we believe, are the correct values to use to predict the topological charge. It is amusing to note that, above the transition (at $m_q=0$), where $\langle\overline{\psi}\psi\rangle$ should vanish at $m_q=0$, the extrapolations at constant $6/g^2$, even where they cross the transition, do better than those where $6/g^2$ is changed to avoid the transition.

We have calculated the topological charge Q on each configuration using the cooling method [17] described in more detail in our earlier paper [1]. From these Q's we have calculated the topological susceptibilities χ as

$$\chi=\frac{1}{V}\langle Q^2\rangle. \tag{10}$$

The values we obtain by applying this method naively at $6/g^2=5.45$ are actually slightly larger at this quark mass ($m_q=0.00625$) than they were at $m_q=0.0125$ [$28(3)\times10^{-5}$ compared with $24(5)\times10^{-5}$] whereas χ should be proportional to m_q and thus smaller at the lower mass. For this reason we have recalculated χ after removing small instantons by hand from the cooled configurations. Here the value at $m_q=0.00625$ has dropped to $19(2)\times10^{-5}$, indicating that small instantons, which are a lattice artifact, are part of the problem, which suggests that the lattice spacing is too large to allow complete separation of long- and short-distance effects on these lattices. The complete results are shown in Table IV, and compared with the theoretical value for the confined region

TABLE IV. Topological susceptibility χ. Standard gives the results obtained by the cooling method. Broad are the results after removing small instantons, i.e., those where the maximum value of $|F\widetilde{F}|$ on a site is $\geqslant 2$.

		$\chi\times10^5$		
$6/g^2$	Cools	Standard	Broad	Theory
5.450	50	28.2(3.4)	19.1(1.9)	11.1(0.5)
5.475	25	19.8(1.9)	12.5(1.2)	—
5.500	50	5.9(1.1)	3.6(0.5)	0.0
5.525	25	5.5(0.9)	2.9(0.7)	0.0
5.550	25	4.0(0.9)	2.1(0.5)	0.0
6.000	25	0.0	0.0	0.0

$$\chi=\frac{m_q}{n_f^2}\frac{n_f}{4}\langle\overline{\psi}\psi\rangle, \tag{11}$$

which is valid for small m_q. We note that, in the hadronic phase at $\beta=5.45$, our measured value is greater than that in theory, as expected. In the plasma phase, we have equated theory to zero since $\langle\overline{\psi}\psi\rangle$ should vanish in the chiral limit in this chirally symmetric phase. The reason χ does not, and should not vanish in this phase, is that the theoretical expression above neglects terms higher order in m_q. In fact, in the plasma phase

$$\chi\propto m_q^{n_f}=m_q^2. \tag{12}$$

At $6/g^2=5.55$, which is above the transition for both masses, $\chi=3.0(6)$ for $m_q=0.0125$ and, even with small instantons removed $\chi=2.1(5)$ at $m_q=0.00625$, a ratio of ≈ 1.4 rather than the predicted four. Further analysis reveals that at least part of this is due to the finite lattice spacing which raises the energy of the ''zero mode'' associated with the instanton to a higher value, comparable in magnitude to the quark mass, invalidating the derivation of this formula [18].

It is worth noting that, in contrast with what has been observed by others for hybrid Monte Carlo simulations [19], the autocorrelation times (in molecular dynamics time) for topological charge and susceptibility we observed in these simulations, which use the hybrid molecular dynamics method with noisy fermions, are not substantially longer than those for other observables. For this reason $(1/V)\langle Q\rangle^2\ll\chi$, which is necessary for a believable measurement of χ. This is in agreement with other simulations using the hybrid molecular dynamics algorithm with noisy fermions [20]. Values of $(1/V)\langle Q\rangle^2$, and these autocorrelation times, are given in Table V. The values we quote for the autocorrelation times are, in fact, the times taken for the autocorrelation function to fall to e^{-2} of its zero-time value, rather than e^{-1} which would be the correct definition if the autocorrelation function were a simple exponential. However, we believe that this is a better estimate in lattice simulations where autocorrelation functions are unlikely to be simple exponentials. Because e^{-2} is comparable to the size of statistical fluctuations in our autocorrelation functions, the values of autocorrelation times in Tables V and VI should only be taken as a rough guide to the size of the true autocorrelation times in these simulations. In Table VI we give values of the autocorrelation times de-

TABLE V. $(1/V)\langle Q\rangle^2$ and estimates of the autocorrelation times for topological charge τ_Q and for χ, τ_χ as functions of $6/g^2$.

$6/g^2$	$\frac{1}{V}\langle Q\rangle^2$	τ_Q	τ_χ
5.450	$0.6(1.8)\times10^{-5}$	35	10
5.475	$1.1(1.3)\times10^{-5}$	35	10
5.500	$0.6(6)\times10^{-5}$	45	45
5.525	$0.09(23)\times10^{-5}$	45	15
5.550	$0.002(25)\times10^{-5}$	40	20

fined as above for the Wilson-Polyakov line $\langle\overline{\psi}\psi\rangle$ and plaquette action for comparison.

We end this section with an estimate of the temperature of the transition from hadronic matter to a quark-gluon plasma. Once we know the critical value of $6/g^2$, the critical temperature T_c is given by

$$T_c=\frac{1}{N_t a(g_c^2)}. \tag{13}$$

The lattice spacing $a(g_c^2)$ can be determined from measurements of the hadron spectrum at zero temperature at $6/g^2=6/g_c^2$. Since this has not been done, we have calculated $a(g_c^2)$, from a value of the ρ mass obtained by interpolation from simulations at other values of $6/g^2$ and m_q, following Blum *et al.* [14]. This yields $T_c=150(9)$ MeV for $m_q=0.0125$, $T_c=140(8)$ MeV for $m_q=0.00625$, and $T_c=128(9)$ MeV at $m_q=0$.

III. SCREENING LENGTHS

In this section we present our measurements of screening masses, the inverse of screening lengths. We measure the correlations of timelike Wilson lines which are related to the string tension in hadronic matter, and the Debye screening length or mass in the quark-gluon plasma, which is the range of influence of a static color charge in the plasma. The correlations of spacelike Wilson lines are also measured. In addition, we measure the screening masses for excitations with the quantum numbers of low-mass hadrons, to determine whether quark-gluon plasma has hadronlike excitations, or whether it is best described in terms of quark and gluon excitations.

As described in [1], we measure correlations between

TABLE VI. Estimates of autocorrelation times for the Wilson-Polyakov line τ_{WL}, the chiral condensate $\langle\overline{\psi}\psi\rangle$, $\tau_{\psi\psi}$, and plaquette $\tau_{\rm plaq}$ as functions of $6/g^2$.

$6/g^2$	τ_{WL}	$\tau_{\psi\psi}$	$\tau_{\rm plaq}$
5.450	17	13	21
5.475	48	39	51
5.500	36	33	23
5.525	31	78	64
5.550	24	25	9
6.000	17	2	3

TABLE VII. Effective masses $\mu(Z)$ from temporal Wilson line correlations.

	Temporal Wilson-Polyakov line effective mass			
$6/g^2$	$Z=0$–1	$Z=1$–2	$Z=2$–3	$Z=3$–4
5.450	1.10(8)	0.84(11)	0.96(26)	1.35(80)
5.475	0.94(4)	0.70(6)	0.73(15)	0.93(46)
5.500	0.70(8)	0.49(9)	0.49(13)	0.57(30)
5.525	0.77(5)	0.60(6)	0.66(13)	0.86(41)
5.550	0.84(7)	0.75(15)	0.91(40)	—
6.000	0.74(4)	0.68(6)	0.66(16)	0.78(41)

''fuzzy'' Wilson-Polyakov loops with zero x, y, and t momenta, correlated in the z direction. Again, we find that those which were ''blocked'' the maximum number of times (3), i.e., maximally ''fuzzy,'' were the most correlated. For timelike Wilson lines our subtracted correlation function should behave at large z separations Z as

$$P(Z)=A\{\exp[-\mu Z]+\exp[-\mu(N_s-Z)]\}. \tag{14}$$

As usual, one obtains effective screening masses $\mu(Z)$ (where we have suppressed the mass dependence) by fitting this form for $P(Z-1)$ and $P(Z)$. Then $\mu(Z)\to\mu$, the screening mass, which is closely related to the Debye screening mass [21]. The screening masses so obtained are tabulated in Table VII. As can be seen, except for the $6/g^2=5.55$ results, our data show some evidence for a plateau as early as the $Z=1$–2 effective masses $[\mu(2)]$, so we use $\mu(2)$ as our estimate for μ. In the plasma phase, the quantity of interest μ/T has the values 3.8(7) at $6/g^2=5.5$, 4.8(5) at $6/g^2=5.525$, 6.0(1.2) at $6/g^2=5.55$, and 5.4(5) at $6/g^2=6.0$, not significantly different from the $m_q=0.0125$ results.

The correlations $C(Z)$ between spatially oriented ''fuzzy'' Wilson-Polyakov lines also have an exponential asymptotic behavior. Unlike the temporal Wilson-Polyakov lines, the spatial lines do not develop a vacuum expectation value corresponding to a perimeter law in the high-temperature phase, but retain an area law defining a confining theory in both phases. The effective masses we obtained from $C(Z)$ for maximal blocking are given in Table VIII. We note that these values are very similar to those at $m_q=0.0125$. Taking $\mu(2)$, the value from fitting $C(Z)$ from $Z=1$ to $Z=2$, as our best estimate of the mass μ, we can extract a string tension $\kappa=\mu/N_t$. Figure 5 shows $\sqrt{\kappa}/m_\rho$ as

TABLE VIII. Effective masses $\mu(Z)$ from spatial Wilson-Polyakov line correlation functions.

	Spatial Wilson-Polyakov line effective mass			
$6/g^2$	$Z=0$–1	$Z=1$–2	$Z=2$–3	$Z=3$–4
5.450	2.80(7)	1.93(43)	—	—
5.475	2.45(6)	1.68(22)	0.91(83)	—
5.500	1.92(5)	1.10(12)	—	—
5.525	1.74(4)	1.19(12)	1.28(34)	—
5.550	1.53(5)	0.97(8)	1.09(31)	—
6.000	0.51(2)	0.41(3)	0.39(3)	0.40(5)

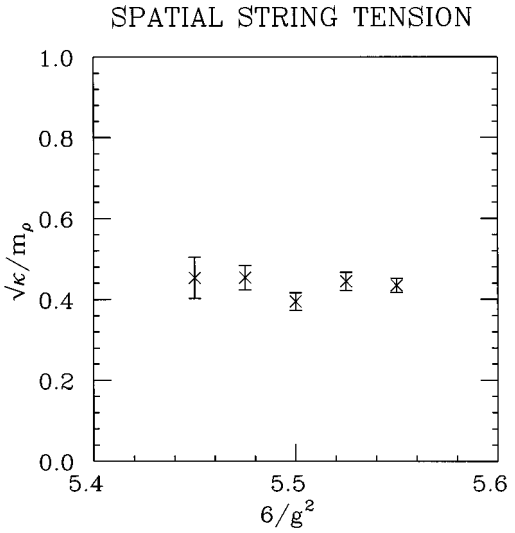

FIG. 5. Spatial string tension κ as a function of $6/g^2$.

a function of $6/g^2$, indicating that the string tension appears to be constant in physical units. This is in accord with expectations that these spatial Wilson lines should show confinement at all temperatures [22].

Let us now turn to the hadron screening lengths, or rather their inverses, the hadron screening masses. Not only can measurements of these screening masses give indications of the nature of excitations in hadronic matter and the quark-gluon plasma, but they can also shed light on the nature of chiral symmetry restoration [23]. A full understanding of chiral symmetry realizations at finite temperature requires a study of the flavor singlet mesons with their disconnected contributions, which is beyond the scope of this paper. However, as we will see, we can at least address some of these issues.

For massless quarks, the $SU(2)_A$ component of the $SU(2)\times SU(2)$ chiral symmetry is spontaneously broken, while the $SU(2)_V$ symmetry is unbroken. The $U(1)_V$ symmetry (baryon or quark number) is conserved, while the $U(1)_A$ is broken explicitly by the chiral anomaly, as well as spontaneously. At the finite-temperature transition, the chiral condensate vanishes, so one expects the $SU(2)_A$ and hence the $SU(2)\times SU(2)$ chiral symmetry to be restored. What is less clear is whether the $U(1)_A$ is restored to give $U(2)\times U(2)$ chiral symmetry [24].

The description of which spatial hadron propagators were considered to get our screening masses was given in our first paper, and will not be repeated here, except to note that wall sources and the $x-y-t$ Coulomb gauge were employed again, the correlations being measured in the z direction. We also measured screening masses for hadronic excitations involving valence ''strange'' quarks whose masses are given above.

Figure 6(a) shows the screening masses of the π and the connected part of the f_0 (σ) propagator, the a_0 propagator. The error bars reflect only statistical errors. These two masses would become equal when $U(1)_A$ symmetry is restored. The π and a_0 appear to have an appreciable mass splitting just above the transition, only approaching each other for considerably higher $6/g^2$. The fact that this splitting appears to be greater than that at $m_q=0.0125$ indicates that finite quark mass is probably not the reason for this splitting. However, since the a_0 mass is difficult to measure we cannot rule out at least part of this splitting being due to systematic errors. More importantly, since flavor symmetry breaking is large at these $6/g^2$ values, we cannot rule out the splitting being due to flavor symmetry breaking. Taken at face value these data suggest that $U(1)_A$ symmetry is not restored at the transition, but instead is restored as $T\to\infty$. Recent measurements of the disconnected part of the f_0 propagator [18], and the susceptibility associated with it [25–27] indicate that it splits the f_0 and a_0 masses in the neighborhood of the transition and gives $f_0-\pi$ degeneracy. This supports the scenario where $SU(2)_A$ is restored at the transition, as expected, but $U(1)_A$ is only restored at somewhat higher temperatures.

The ρ and a_1 screening masses as a function of $6/g^2$ are presented in Fig. 6(b). Since these states lie in the same $SU(2)\times SU(2)$ multiplet, their masses should become equal when $SU(2)_A$ is restored. What we observe is that these screening masses do come together just above the transition indicating that $SU(2)\times SU(2)$ is restored at the transition, in the chiral limit. Similarly, Fig. 6(c) indicates that the N and N' (negative-parity nucleon) become degenerate at (or near) the transition which is also evidence that chiral $SU(2)\times SU(2)$ symmetry is restored.

We also note that, just above the transition, the ρ and a_1 masses lie just below the energy of two free quarks at the lowest Matsubara frequency, i.e., $2\pi T$, and presumably approach this value from below as $T\to\infty$. Similarly, the N and N' masses lie just below the energy of three free quarks at the lowest Matsubara frequency ($3\pi T$), and approach this value at high temperatures. Thus these states appear to be weakly bound above T_c. In contrast, both the π and the a_0 masses are considerably below $2\pi T$, just above the transition, only approaching this limit as $T\to\infty$, indicating that they remain strongly bound, even in what is usually thought of as the deconfined phase. Thus the quark-gluon plasma does appear to support hadronic excitations.

Finally in Fig. 6(d), we present our kaon screening lengths for the choices of the valence strange quark mass given above. The pion screening lengths are given for comparison. Note that the pion screening mass is for $m_{u,d}=0.00625$ which is considerably larger than the physical quark mass, so that the pion screening masses will be too large. However, the strange quark masses are tuned to give reasonable values for the kaon mass, so that kaon screening lengths we obtained should be reasonable estimates for the physical kaon screening lengths.

IV. DISCUSSION AND CONCLUSIONS

We have extended our previous simulations of the thermodynamics of lattice QCD with two light-staggered quarks down to quark mass $m_q=0.00625$ (lattice units), in an attempt to probe the chiral limit. At this mass we find a transition at a critical coupling, $6/g_c^2=5.49(2)$, corresponding to a critical temperature $T_c=140(8)$ MeV. Combining this with our previous result at $m_q=0.0125$, we predict a critical coupling given by $6/g_c^2=5.44(3)$ corresponding to $T_c=128(9)$ MeV in the chiral ($m_q=0$) limit. As expected, there is no evidence for a first-order transition.

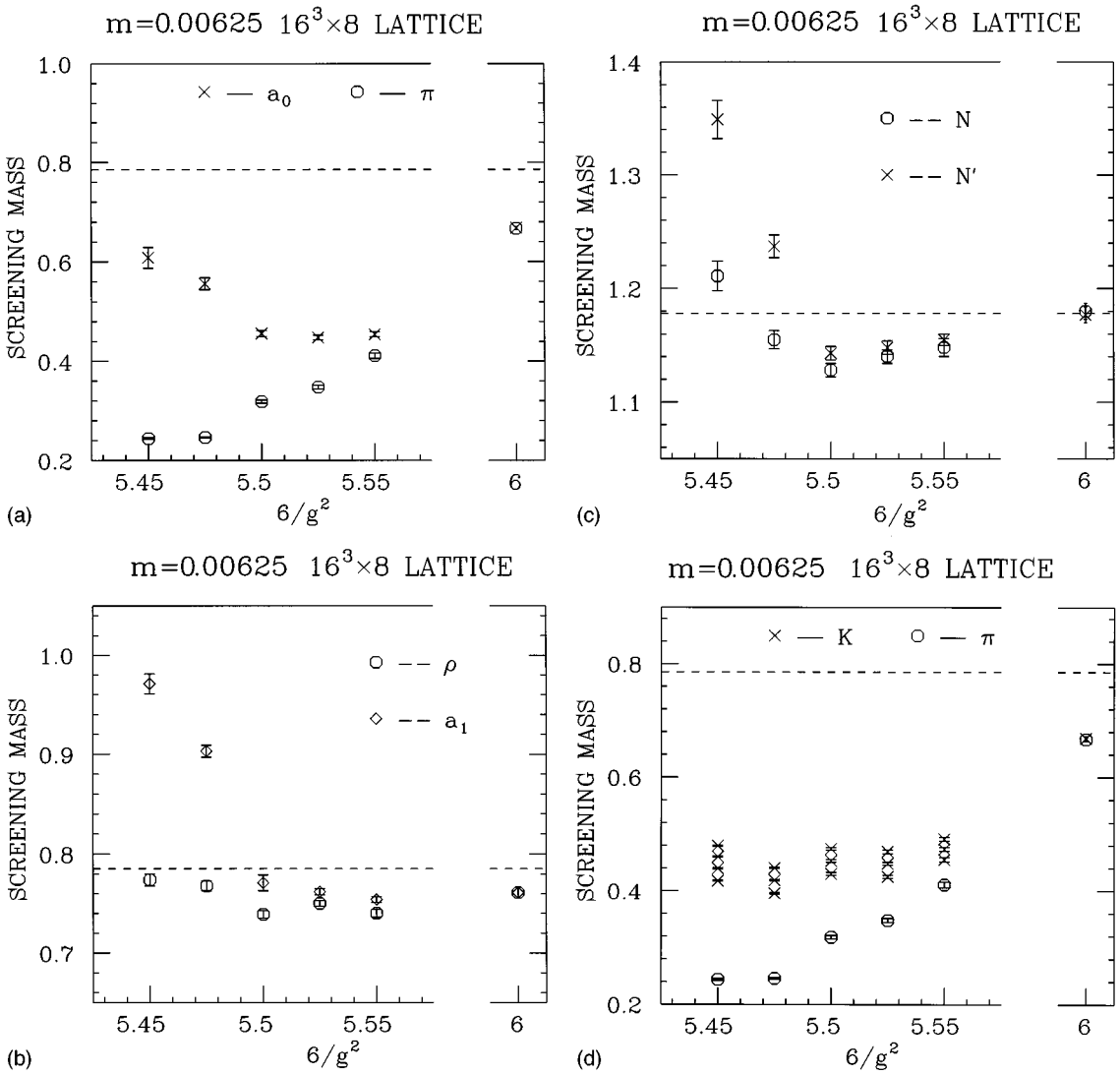

FIG. 6. Hadronic screening masses as functions of $6/g^2$: (a) Scalar states, π, a_0, (b) vector states, ρ, a_1, (c) nucleon states, N, N', (d) K, π.

The screening length associated with thermal Wilson-Polyakov line correlations is quantitatively similar to that obtained from our published $m_q=0.0125$ calculations. Thus our conclusion that we should expect ψ/J suppression for $T\gtrsim 2T_c$ still stands, while the situation for $T_c<T\lesssim 2T_c$ remains unclear.

We observed that the entropy of strange quarks is $\sim 70\%$ of that of either u or d quarks, just above the transition. It is to be hoped that phenomenology based on this number might shed light on whether there is an increase in kaon production as the system passes through this transition.

Our study of hadron screening lengths indicates that the π, K, and a_0 states remain strongly bound above the transition. Thus there are excitations with these quantum numbers (and presumably those of the f_0), in the quark-gluon plasma. Such binding is presumably related to the finite string tension we have observed in our spatial Wilson line correlations. The other hadronic excitations we observed (ρ, a_1, N, and N') appear to be only weakly bound above the transition. The relatively large separation of the π and a_0 masses above the transition compared with that of the ρ and a_1 suggests that these do not become degenerate at the transition, so that the restored symmetry above the transition is $SU(2)\times SU(2)\times U_V(1)$ rather than $U(2)\times U(2)$ as some have suggested. This is in agreement with recent calculations of the chiral susceptibility χ_m, and calculations of the f_0 mass from the full (connected + disconnected) propagator.

Our calculation of the baryon-number susceptibility gives us a glimpse of physics at finite baryon number density. Calculation of topological susceptibility at this low mass appears to be strongly affected by the large lattice spacing at T_c, preventing us from reliably extracting its mass dependence.

For the standard Wilson action which we used, we need a larger value of N_t to remove finite lattice spacing effects. We also need a larger aspect ratio (N_s/N_t) to make finite lattice-size correction factors closer to 1, reducing the systematic uncertainties in extracting entropy densities, energy densities, and pressures. The larger N_s is also needed to reduce the systematic errors involved in extracting screening lengths. Zero-temperature values of the plaquette observable and $\langle\overline{\psi}\psi\rangle$ are needed to extract partial pressures and energy den-

sities. Measurements closer together in $6/g^2$ will be necessary if we are to extract the fluctuation quantities involved in obtaining the equation of state.

ACKNOWLEDGMENTS

The computations were carried out on the Connection Machine CM-2 at the Pittsburgh Supercomputing Center, under an NSF grand challenge allocation. This work was supported by the U. S. Department of Energy under Contract No. W-31-109-ENG-38, and Grant Nos. DE-FG02-91ER-40661, DE-FG05-92ER-40742, DE-FG05-85ER250000, and DE-FG03-95ER-40906, and the National Science Foundation under Grant Nos. NSF-PHY91–16964, NSF-PHY-9503371, and NSF-PHY92-00148. S.K. was supported by KOSEF through CTP.

[1] The HTMCGC Collaboration, S. Gottlieb *et al.*, Phys. Rev. D **47**, 3619 (1993).
[2] The HTMCGC and HEMCGC Collaborations, K. M. Bitar *et al.*, in *Lattice '92*, Proceedings of the International Symposium, Amsterdam, The Netherlands, edited by J. Smit and P. van Baal [Nucl. Phys. B (Proc. Suppl.) **30**, 315 (1993)].
[3] HTMCGC and MILC Collaborations, C. Bernard *et al.*, in *Lattice '94*, Proceedings of the International Symposium, Bielefeld, Germany, edited by F. Karsch *et al.* [Nucl. Phys. B (Proc. Suppl.) **42**, 448 (1995)].
[4] R. D. Mawhinney, in *Lattice '92* [2], p. 331.
[5] S. Gottlieb *et al.*, Phys. Rev. Lett. **59**, 1513 (1987); F. R. Brown *et al.*, *ibid.* **65**, 2491 (1990); M. Fukugita *et al.*, *ibid.* **65**, 816 (1990).
[6] C. Bernard *et al.*, Phys. Rev. D **45**, 3854 (1992).
[7] C. Bernard *et al.*, Phys. Rev. D **54**, 4585 (1996).
[8] R. Pisarski and F. Wilczek, Phys. Rev. D **29**, 338 (1984).
[9] F. Karsch, Nucl. Phys. **B205**, 285 (1982); F. Karsch and I. O. Stamatescu, Phys. Lett. B **227**, 153 (1989).
[10] J. Engels, F. Karsch, and H. Satz, Nucl. Phys. **B205**, 239 (1982).
[11] P. Mackenzie (private communication).
[12] S. Gottlieb *et al.*, Phys. Rev. Lett. **59**, 2247 (1987); Phys. Rev. D **38**, 2888 (1988).
[13] F. Karsch and E. Laermann, Phys. Rev. D **50**, 6954 (1994).
[14] T. Blum *et al.*, Phys. Rev. D **51**, 5153 (1995).
[15] A. M. Ferrenberg and R. H. Swendsen, Phys. Rev. Lett. **61**, 2635 (1988); **63**, 1658 (1989).
[16] J.-F. Lagaë (private communication).
[17] M. Teper, Phys. Lett. **162B**, 357 (1985); J. Hoek, M. Teper, and J. Waterhouse, Nucl. Phys. **B288**, 589 (1987).
[18] J. B. Kogut, J.-F. Lagaë, and D. K. Sinclair, in *Lattice '96*, Proceedings of the International Symposium, St. Louis, Missouri, edited by C. Bernard *et al.* [Nucl. Phys. B (Proc. Suppl.) **53**, 269 (1997)].
[19] G. Boyd *et al.*, in *Lattice '96* [18], p. 544.
[20] K. M. Bitar *et al.*, Phys. Rev. D **44**, 2090 (1991); K. M. Bitar *et al.*, in *Lattice '92* [2], p. 315.
[21] N. Attig *et al.*, Phys. Lett. B **209**, 65 (1988); A. Irbäck *et al.*, Nucl. Phys. **B363**, 34 (1991).
[22] E. Manousakis and J. Polyoni, Phys. Rev. Lett. **58**, 847 (1987).
[23] C. DeTar and J. B. Kogut, Phys. Rev. Lett. **59**, 399 (1987); Phys. Rev. D **36**, 2828 (1987).
[24] E. Shuryak, Comments Nucl. Part. Phys. **21**, 235 (1994).
[25] MILC Collaboration, C. Bernard *et al.*, in *Lattice '96* [18], p. 442; MILC Collaboration, C. Bernard *et al.*, Phys. Rev. Lett. **78**, 598 (1997).
[26] G. Boyd *et al.*, Report No. hep-lat/9607046, 1996 (unpublished).
[27] N. H. Christ, in *Lattice '96* [18], p. 253.